Pergamon

Int. J. Heat Mass Transfer. Vol. 37, No. 11, pp. 1641–1655, 1994

0017-9310/94 $7.00+0.00

0017-9310(93)0099-3

Liquid microlayer evaporation during nucleate boiling on the surface of a flat composite wall

ZHANXIONG GUO and MOHAMED S. EL-GENK

Institute for Space Nuclear Power Studies, Department of Chemical and Nuclear Engineering, University of New Mexico, Albuquerque, NM 87131, U.S.A.

(*Received* 5 *January* 1993 *and in final form* 24 *November* 1993)

Abstract—A transient model is developed to study the evaporation of a liquid microlayer under a growing vapor bubble during nucleate boiling on the surface of a flat composite wall. The wall consists of a thin, volumetrically heated metallic foil or film and a Pyrex glass substrate or thin coating. The model predictions are qualitatively in agreement with experimental data for a water microlayer evaporation on a SnO_2 coated Pyrex glass plate. Results for a heated metal foil on a Pyrex glass substrate show that the local heat flux at the solid–liquid–vapor triple point could be as much as one to two orders of magnitude higher than the input heat flux. Consequently, the wall temperature at the triple point drops rapidly, resulting in a non-uniform wall surface temperature. Both the accommodation coefficient of evaporation and lateral heat conduction in the heated wall significantly affects the liquid microlayer evaporation on a thin, highly conductive wall, especially during the early stage of the bubble growth. As either the thickness or the thermal conductivity of the heated wall is increased, the evaporation rate increases due to improved lateral heat conduction, approaching that for an isothermal wall. Conversely, a thin coating of low conductivity material significantly reduces the evaporation rate of the liquid microlayer, whereas the effect of the thermal properties of the heated metallic substrate is negligible unless the coating is very thin.

1. INTRODUCTION

IN SEARCH of an explanation to the high heat transfer rate associated with nucleate boiling, a liquid layer evaporation model was first proposed by Snyder and Edward [1]. The model attributes a significant portion of the total heat transfer rate in boiling to the rapid evaporation of a thin liquid film (or microlayer) which forms underneath a growing vapor bubble on a heated surface. The first indirect experimental observation indicating microlayer formation in nucleate boiling was made by Moore and Mesler [2]. They observed a rapid drop in the temperature of the heated surface during a bubble growth and a temperature recovery after the bubble departed. Simultaneous visualization of vapor bubble growth and surface temperature measurement was made by Rogers and Mesler [3]. They indicated that the drop in the surface temperature associated with a bubble growth implies a rapid evaporation of a liquid microlayer beneath the growing bubble. Similar observations were also made by Cooper and Lloyd [4].

Direct measurements of the microlayer thickness (usually less than 10 μm) by means of optical interferometry were made by Sharp [5] and Voutsinos and Judd [6]. Most recently, Koffman and Plesset [7] measured the time history of the microlayer thickness for nucleate boiling of water and ethanol using laser interferometry, combined with high speed photography. Their experimental results showed that the liquid microlayer was almost wedge shaped and as the bubble grew in size, the microlayer thickness decreased and the radius of the dry spot forming underneath the bubble increased. Koffman and Plesset attributed the reduction in the microlayer thickness with time solely to liquid evaporation and concluded that radial flow of liquid into the microlayer was negligible. This conclusion was consistent with an earlier suggestion by Cooper and Lloyd [8].

A number of analytical and numerical investigations have been carried out to elucidate the effects of the thermal–physical properties and the thickness of the heated wall on the evaporation of a thin liquid layer. Hale and Anderson [9] studied the evaporation of a thin liquid film, having a uniform thickness, on a heated flat plate. Their numerical results showed that the time needed for the thin liquid film to completely evaporate depends on the thermal conductivity and heat capacity of the underlying wall. The effect of the wall thickness on nucleate boiling was investigated numerically by Prasad *et al.* [10]. They modeled the heat conduction through a liquid macrolayer, which was an order of magnitude thicker than a microlayer, ignoring not only the variation in the liquid film thickness due to non-uniform evaporation, but also the effect of the solid–liquid–vapor (s–l–v) triple point. They found that the heat transfer rate through the macrolayer depends on the wall thickness, but only within a certain range.

The effect of the s–l–v triple point and the thermal conductivity of an isothermal wall on the heat transfer rate during condensation was studied analytically by Brown and Martin [11]. They found the heat flux at the triple point to be very high, limited only by the

NOMENCLATURE

a	accommodation coefficient of evaporation
c	specific heat [J kg^{-1} K^{-1}]
h	heat transfer coefficient [W m^{-2} K^{-1}]
h_{fg}	latent heat of vaporization [J kg^{-1}]
k	thermal conductivity [W m^{-1} K^{-1}]
M	molecular weight of the boiling liquid [kg kmol^{-1}]
p	system pressure [N m^{-2}]
q''	heat flux [W m^{-2}]
q'''	volumetric heat generation rate [W m^{-3}]
R	radius of the heated wall [m]
$\Re$	universal gas constant [J kmol^{-1} K^{-1}]
R_b	maximum bubble radius [m]
r_d	radius of the dry spot under a bubble [m]
s	thickness [m]
t	time [s]
T	temperature [K]
T_o	initial solid–liquid interface temperature [K]
t_g	growth time of a vapor bubble [s]
t_w	waiting period for bubble nucleation [s].

Greek symbols

δ	microlayer thickness [m]
ρ	density [kg m^{-3}]
Θ	dimensionless temperature, $[(T-T_{sat})/(T_o-T_{sat})]$.

Subscripts

1	coating, or upper wall region
2	substrate
e	evaporation
l	liquid
ls	liquid–solid interface
lv	liquid–vapor interface
sat	saturation
v	vapor.

finite conductivity of the underlying metallic wall and the liquid–vapor interfacial resistance. Using a high thermal conductivity wall improved lateral flow of heat towards the region of the triple point, resulting in a significant increase in the overall heat transfer coefficient. Although this analysis demonstrated the importance of the triple point on the overall heat transfer rate during condensation, the results are not directly applicable to microlayer evaporation during nucleate boiling. In their analysis, Brown and Martin [11] assumed the thermal–physical properties of the wall and the thickness of the condensate layer, which was much thicker than the microlayer in nucleate boiling [7], to be constant and the triple point to remain stationary. On the other hand, the liquid microlayer forming beneath a growing vapor bubble, in addition to being extremely thin, has thickness and evaporation rate which are non-uniform. Furthermore, the triple point moves outward with time due to the dry out of the liquid microlayer beneath the bubble [7].

Recently, Guo and El-Genk [12] investigated numerically the liquid microlayer evaporation in nucleate boiling and determined the effects of the thermal physical properties and the heating method (isoflux heating and volumetric heat generation) of the heated wall. Results indicated that the microlayer evaporation increased with the wall thermal diffusivity, but was almost independent of the heating method of the wall. Results also showed that the wall heat flux at the triple point could be as much as one to two orders of magnitude higher than the input heat flux, depending on the value of the accommodation coefficient of evaporation.

Although in most experiments investigating microlayer evaporation the heated wall consisted basically of a thin, volumetrically heated metal foil or a metallic film underlaid by a low thermal conductivity substrate (e.g. Pyrex glass), previous models ignored the effect of the wall and the substrate. The objective of this work is to extend the work of Guo and El-Genk [12] to numerically investigate the evaporation of a liquid microlayer on a flat surface of a composite wall. The wall consists of a thin, volumetrically heated metallic foil or film and a Pyrex glass substrate or thin coating. A transient model, which thermally couples the wall regions with the evaporating microlayer, is developed to simulate microlayer evaporation during bubble growth as observed in the experiments of Koffman and Plesset [7]. In addition, a parametric analysis is performed to investigate the effects of the thickness and material properties of the wall regions, the value of accommodation coefficient of evaporation, and the waiting period between successive bubbles on the microlayer evaporation. Also, the effect on the evaporation rate of the microlayer of applying a thin Pyrex glass coating on the surface of a metallic, volumetrically heated substrate is investigated.

2. GOVERNING EQUATIONS

A schematic diagram of an evaporating liquid microlayer, as observed in nucleate boiling at low heat flux [7], on the surface of a flat composite wall is depicted in Fig. 1(a). The corresponding solution domain used in the numerical calculation (Fig. 1(b)) is divided into four subdomains: the vapor, the liquid microlayer, and the upper and lower wall regions. Also shown in Fig. 1 are the parameters and coor-

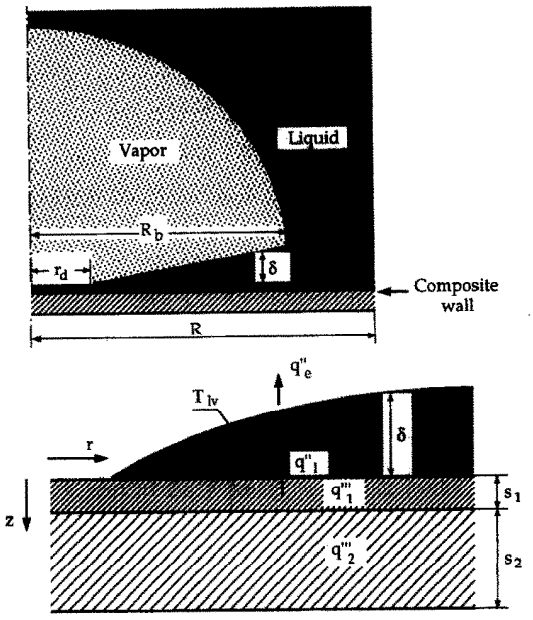

FIG. 1. Schematic of a microlayer.

dinates that define the geometry of the problem. In formulating the problem, the following simplifying assumptions are made:

(1) Prior to the nucleation of a bubble at a given site, the temperatures of the surface and in both regions of the wall are determined using 1-D steady-state axial conduction and assuming nucleate boiling heat transfer at the surface [13].

(2) During the bubble growth, heat transfer in the wall is treated as a two-dimensional, transient conduction problem subjected to an adiabatic boundary condition at its outer radius ($r = R$).

(3) Since the liquid microlayer is sufficiently thin (<10 μm), lateral liquid flow and heat convection in the microlayer are neglected. The change in the liquid microlayer thickness with time is only due to evaporation [8].

(4) Because of the low thermal conductivity of the liquid, radial conduction is negligible, and hence the heat flow in the microlayer is governed by axial heat conduction.

(5) Thermal capacity of the microlayer is negligible compared to the latent heat of vaporization.

(6) Heat transfer between the wall and the vapor space above the dry spot, which forms underneath the growing bubble, is neglected due to the low surface temperature.

(7) The properties of the wall materials and the liquid in the microlayer are evaluated at the liquid saturation temperature at atmospheric pressure.

2.1. *Heat transfer in the wall*

The energy equations and the appropriate boundary and initial conditions in the wall are developed in a cylindrical coordinate system shown in Fig. 1. Although the governing equations described are for a dual-layered wall, they are coded such that the selection of a single wall system can be made in the input file.

Energy equation

The energy equation in the wall can generally be expressed as:

$$\rho_i c_i \frac{\partial T_i}{\partial t} = \nabla (k_i \nabla) T_i + q'''_i, \tag{1}$$

where $i = 1, 2$ denote the upper wall region and the substrate, respectively. This equation is subject to the following boundary conditions.

$$\left[\frac{\partial T_i}{\partial r}\right]_{(r=0,z)} = 0, \text{and} \left[\frac{\partial T_i}{\partial r}\right]_{(r=R,z)} = 0. \tag{2a}$$

The boundary condition at the wall surface ($z = 0$) is given as follows:

$$\left[-k_1 \frac{\partial T_1}{\partial z}\right]_{(r,z=0)} = \begin{cases} 0 & 0 \leqslant r \leqslant r_d \\ q''_{ls} & r_d < r \leqslant R_b \\ h(T_1 - T_{sat}) & R_b < r \leqslant R \end{cases} \tag{2b}$$

and at the bottom surface of the wall is:

$$\left[\frac{\partial T_2}{\partial z}\right]_{(r,z=s_1+s_2)} = 0. \tag{2c}$$

The temperature and heat flux continuity at the interface between the two wall regions ($z = s_1$) yields:

$$T_1(r, z = s_1) = T_2(r, z = s_1), \tag{2d}$$

and

$$\left[k_1 \frac{\partial T_1}{\partial z}\right]_{(r,z=s_1)} = \left[k_2 \frac{\partial T_2}{\partial z}\right]_{(r,z=s_1)}. \tag{2e}$$

The initial condition in the heated wall is given as

$$T(z, r, t = 0) = f(z). \tag{3}$$

In equation (3), $f(z)$ is obtained from the solution of a one-dimensional steady-state form of equation (1) in the axial direction and assuming nucleate boiling of saturated liquid at the wall surface ($z = 0$). The nucleate boiling heat transfer coefficient for water is computed from the formulation of Jacob and Hawkins [13]:

$$h = 5.565[T_{ls}(r,t) - T_{sat}]^3, \tag{4}$$

where $T_{ls}(r,t) = T_1(r, z = 0, t)$.

2.2. *Heat transfer in the liquid microlayer*

The assumptions (3) and (5) above imply that the temperature profile in the microlayer is linear. Therefore the heat flux at the solid–liquid interface ($z = 0$) can be simply given as:

$$q''_{ls}(r,t) = k_1 \frac{T_{ls}(r,t) - T_{lv}(r,t)}{\delta(r,t)}, \tag{5}$$

where $T_{lv}(r,t)$ is the local temperature at the liquid–

vapor interface and $\delta(r,t)$ is the local microlayer thickness. The value of $T_{lv}(r,t)$, which depends on the liquid evaporation at the liquid–vapor interface, is determined in the next section.

2.3. *Evaporation at the liquid–vapor interface*

Due to the interfacial thermal resistance at the liquid–vapor interface, the liquid–vapor interfacial temperature, $T_{lv}(r,t)$, is higher than the corresponding liquid saturation temperature at the local vapor pressure. In order to determine this interfacial temperature, the theoretical evaporation heat transfer rate equation of Hsu and Graham [14], derived from the kinetic theory, is used:

$$q''_e = ah_{fg}\left[\frac{M}{2\pi\Re T_{sat}}\right]^{1/2}[p(T_{lv})-p(T_{sat})]. \quad (6)$$

The evaporation heat flux at the liquid–vapor interface given in equation (6) can also be expressed in terms of the temperature drop across the liquid–vapor interface. In doing so the Clausius–Clapeyron equation

$$\frac{p(T_{lv})-p(T_{sat})}{T_{lv}-T_{sat}} = \frac{\rho_v h_{fg}}{T_{sat}} \quad (7)$$

is used assuming that $[p(T_{lv})-p(T_{sat})]$ is small. Substituting equation (7) into equation (6) yields the following expression for the heat flux at the liquid vapor interface:

$$q''_e = a\rho_v h_{fg}^2\left[\frac{M}{2\pi\Re T_{sat}^3}\right]^{1/2}[T_{lv}-T_{sat}]. \quad (8)$$

Because the thermal capacity of the liquid microlayer is negligible, q''_l can be considered equal to q''_e. By substituting equation (5) into equation (8) and rearranging, the following equation for the local heat flux through the liquid microlayer is obtained.

$$q''_{ls}(r,t) = q''_e(r,t) = \frac{T_{ls}(r,t)-T_{sat}}{\dfrac{\delta(r,t)}{k_l}+\dfrac{1}{a\rho_v h_{fg}}\left[\dfrac{2\pi\Re T_{sat}^3}{M}\right]^{1/2}}. \quad (9)$$

In Equation (9), the first term in the denominator represents the thermal resistance of the liquid microlayer and the second term, which represents the liquid–vapor interfacial thermal resistance, is inversely proportional to the value of the accommodation coefficient of evaporation, a. The value of this coefficient varies widely from 0.04 to 1.0 according to Hsu and Graham [14]. With the thermal capacity and the radial liquid flow in the microlayer being neglected, the radial variation in the microlayer thickness at any instant is calculated from a simple energy balance as follows:

$$\frac{d\delta}{dt} = -\frac{q'''_{ls}}{\rho_l h_{fg}}, \quad (10)$$

where the initial microlayer thickness,

$$\delta(r,0) = g(r) \quad \text{for} \quad 0 \leqslant r \leqslant R_b \quad (11)$$

is an input to the model and can be determined from experiments [7].

3. METHOD OF SOLUTION

Solving the above described system of nonlinear, coupled equations analytically is unattainable without further simplifications of the problem. Instead, a numerical solution of the problem is developed. The governing equations are discretized following the methodology described in ref. [15]. In this solution the vapor subdomain is treated as a single control volume at the saturation temperature corresponding to the system pressure. Since a one-dimensional axial conduction is considered in the liquid subdomain, this domain is discretized only in the radial direction, consistent with the discretization of the heated wall. Discretization of the upper wall region and the substrates are accomplished by dividing them into a number of control volumes of different sizes. The finite difference equations are derived by integrating the differential equations over each control volume.

The resulted finite difference equations are solved iteratively at each time step using Line SOR (Successive Over Relaxation), a semi-implicit method. Each domain is solved successively until a preset convergence criterion is met. An energy balance check is performed in each run to ensure the validity of the results. The calculated error in the overall heat balance can reach as high as 6% at the beginning of the microlayer evaporation process but decreases to less than 2% by the end of a millisecond. It is concluded that an error of this magnitude will not affect the conclusions to be made based on the numerical results.

4. RESULTS AND DISCUSSION

Calculations are performed using different wall composition, materials and thicknesses. The numerical output includes the two-dimensional temperature distributions in the wall regions, the local surface heat flux, the variation in the radial profile of the microlayer thickness and the dry spot radius as a function of time. In all calculations, the wall radius, R, is taken equal to 2.0 mm.

4.1. *Model comparison with experimental results*

In their experiments, Koffman and Plesset [7] used tin oxide (SnO_2) coated Pyrex glass plates as the boiling surface. Since the SnO_2 film is essentially transparent, the changes in the evaporating microlayer thickness and the growth of the dry spot underneath the growing vapor bubble were recorded from the bottom of the composite wall using the optical inter-

ferometry method and a high speed movie camera. A nominally uniform surface heat flux was obtained by passing electrical current through the thin SnO_2 film. According to Koffman and Plesset the Pyrex glass substrate had a thickness of 3.2 mm but the thickness of the SnO_2 film was not measured. Therefore, in simulating the microlayer evaporation in Koffman and Plesset experiments the SnO_2 film thickness is varied as a parameter. Also, a value of 0.04 for the accommodation coefficient of evaporation and a maximum bubble radius of 1.0 mm are assumed.

The liquid microlayer thickness and the bubble radius as functions of time during the early stage of the bubble growth are obtained from the experimental results of Koffman and Plesset [7]. The bubble radius is assumed to remain unchanged after the bubble reaches its maximum radius. Although the liquid in Koffman and Plesset experiments were subcooled, liquid subcooling will insignificantly affect the microlayer evaporation since it is small compared to the latent heat of evaporation. Therefore, all the calculations are performed assuming saturated bulk liquid. The volumetric heat generation rate in the SnO_2 layer is determined by equating the average surface heat flux, $s_1 q_1'''$, in the calculations to the measured value by Koffman and Plesset, $2.04 \times 10^5\ \mathrm{W\,m^{-2}}$. Since the transient growth of the dry spot forming underneath a growing vapor bubble is directly related to the microlayer evaporation rate, the radius of the dry spot, r_d, is used as a parameter in presenting the results of the calculations.

In Fig. 2 the calculated radii of the dry spot as functions of time for several SnO_2 film thickness, are compared with the experimental measurements of Koffman and Plesset [7]. While all curves show the same trend, the one with a SnO_2 film thickness of 30 microns gives the best match with the experimental results. This figure also shows that varying the SnO_2 film thickness from 25 to 35 microns results in only about $\pm 5\%$ change in the numerical predictions of r_d. Figure 3 compares the computed radial profiles of the liquid microlayer thickness at different times during the bubble growth with the experimental measurements for SnO_2 film thickness of 30 microns. These results again show a qualitative agreement between the present model and the experimental measurements of Koffman and Plesset [7]. The model predictions of the microlayer thickness are generally higher than the experimental values and the difference increases with evaporation time. Such a difference between calculations and experiments might be attributed to the effect of successive bubble nucleation from the same site on the temperature filed in the wall. This effect is investigated in the next section.

4.2. *Effect of successive nucleation of vapor bubbles*

According to Koffman and Plesset [7], the average waiting period between a bubble departure and the nucleation of the next bubble from the same nucleation site was about 70 ms. This long waiting period is perhaps due to the liquid subcooling in the experiments (21.7 K). In order to determine the effect of a departing bubble on the microlayer evaporation for the succeeding bubble, calculations are made of the growth of the dry spot beneath the bubble by varying the length of the waiting period. Also, the temperature fields in the wall regions are calculated, both during the growth of the first bubble and the

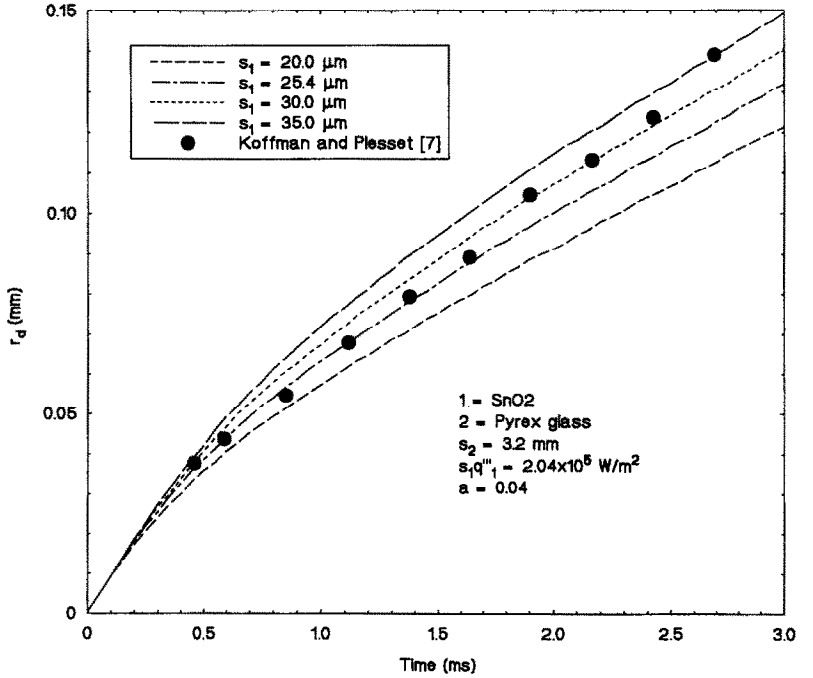

FIG. 2. Comparison of model predictions of dry spot radius with experiments [7].

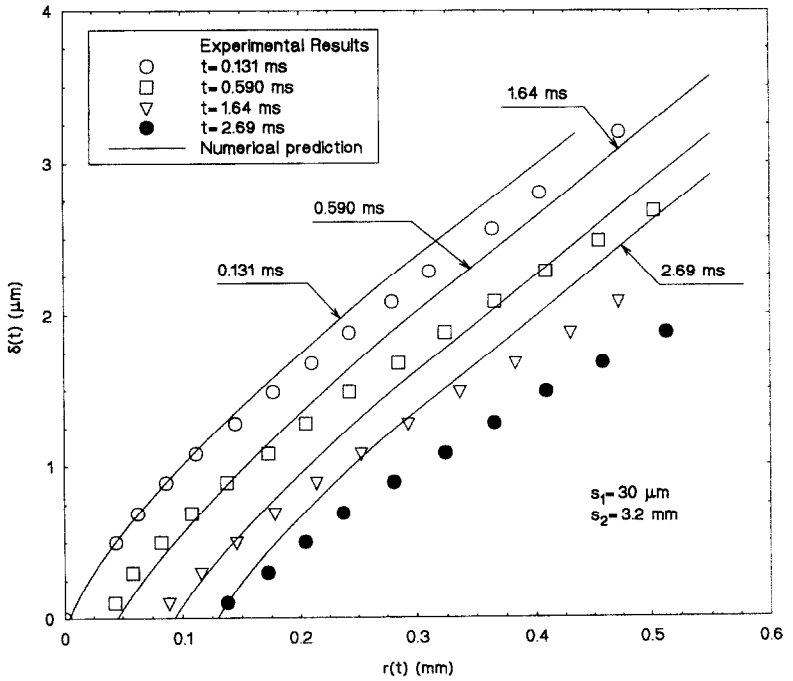

FIG. 3. Comparison of model predictions of microlayer profiles with experiments [7].

waiting period before the nucleation of the next bubble.

Figure 4 shows the radii of dry spots beneath the first and second growing bubbles of different waiting periods. Note that the first bubble is identical to a second bubble of a waiting period of infinity. As this figure indicates, the radius of the dry spot for the second bubble is almost independent of the length of the waiting period for a waiting period of greater than 25 ms and a growth time of less than 1 ms. For a longer growth time, increasing the waiting period allows the temperature field in the wall to recover, which slightly increases the growth rate of the dry spot, and hence the evaporation rate of the liquid microlayer. Figure 5 presents a detailed temperature distribution within the heated SnO_2 film and the Pyrex glass substrate at

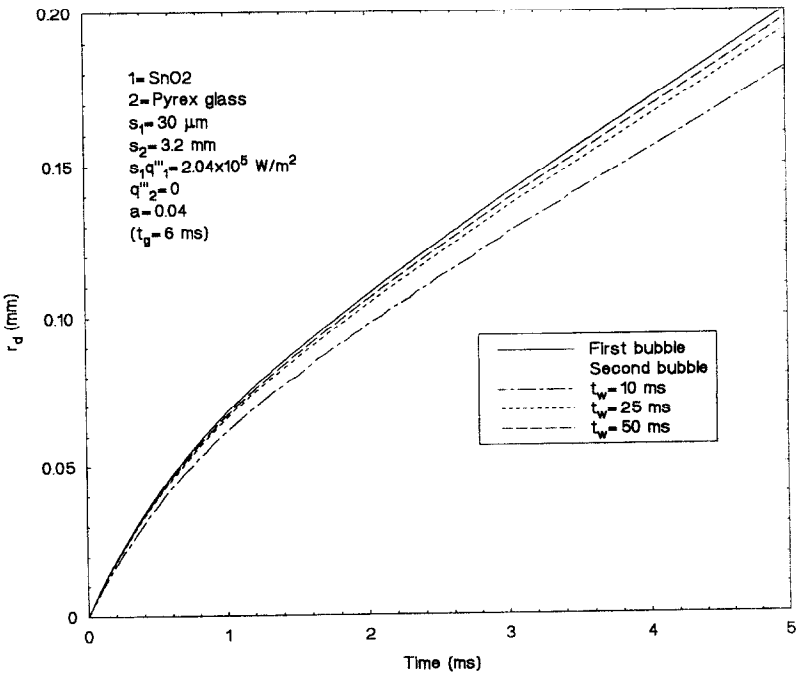

FIG. 4. Effect of the waiting period on the dry spot growth of a successive bubble.

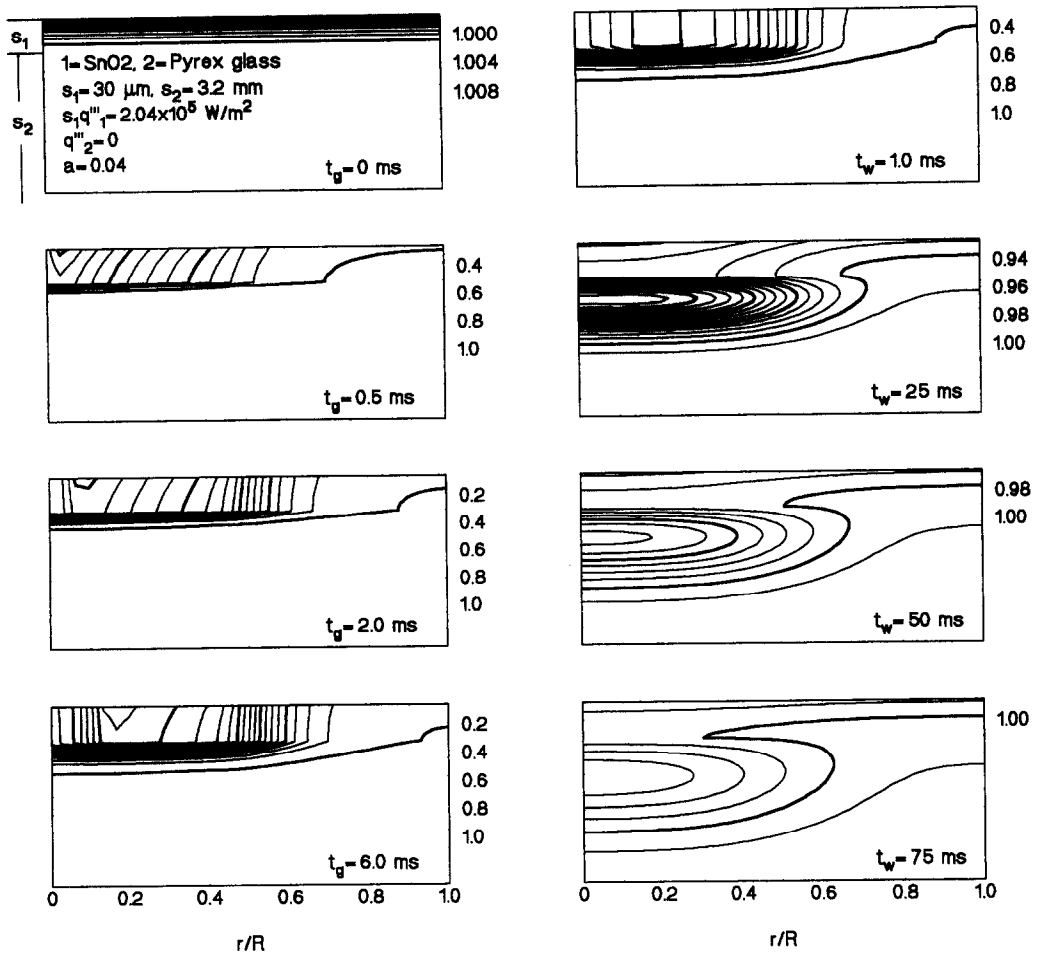

FIG. 5. Variation of temperature field in the heated wall before and after a bubble departure.

different times before and after the departure of the first bubble. As this figure shows, the change in the temperature field in the wall regions is noticeable as the waiting period increases.

In summary, the results suggest that successive bubble nucleation insignificantly affects the microlayer evaporation during nucleate boiling as long as the waiting period is not shorter than about 25 ms. Although the qualitative agreement between the numerical results and the measurements of Koffman and Plesset [7] is not necessarily an indication that all simplifying assumptions are applicable, it demonstrates the validity of the modeling approach. In the following sections, the model is used to study some of the heat transfer aspects of microlayer evaporation on the surface of a composite wall. Numerical results presented are all based on the same initial microlayer thickness and the bubble growth rate and maximum radius as those used when comparing with the experiments of Koffman and Plesset [7].

4.3. *Effect of the accommodation coefficient of evaporation*

In order to quantify the effect of the accommodation coefficient of evaporation numerical calculations are performed of the microlayer evaporation on the surface of a metal foil on a low thermal conductivity substrate. The results for heated metal foils (25.4 μm thick) of largely different thermal properties (stainless-steel and copper) on a 1.0 mm thick Pyrex glass substrate are presented in Figs. 6 and 7. The results show that the evaporation rate is highly nonuniform along the surface of the liquid microlayer. It is very high at the s–l–v triple point, but decreases rapidly with radial distance from the triple point. The evaporation rate at the triple point as well as the change in its value with radial distance increases as the accommodation coefficient of evaporation increases. The effect of the accommodation coefficient on the evaporation heat flux at the triple point is significant, where the microlayer is very thin, but tends to diminish with distance from the triple point as the microlayer thickness increases.

A comparison of Figs. 6 and 7 also shows that the local evaporation heat flux is less sensitive to the value of the accommodation coefficient of evaporation when a stainless-steel foil is used instead of a copper foil, which has a higher thermal conductivity. In the case of stainless-steel, the thermal resistance of the wall dominates the overall heat transfer, and hence

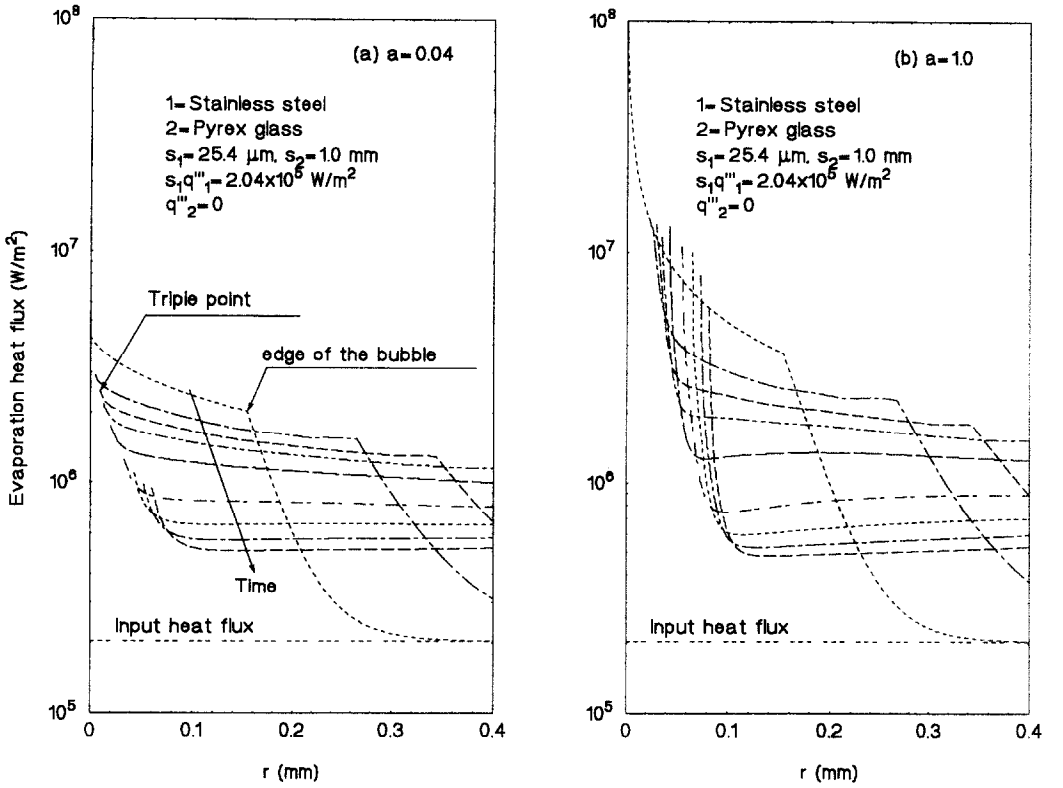

FIG. 6. Effect of the accommodation coefficient of evaporation on the evaporation heat flux on a heated stainless-steel wall.

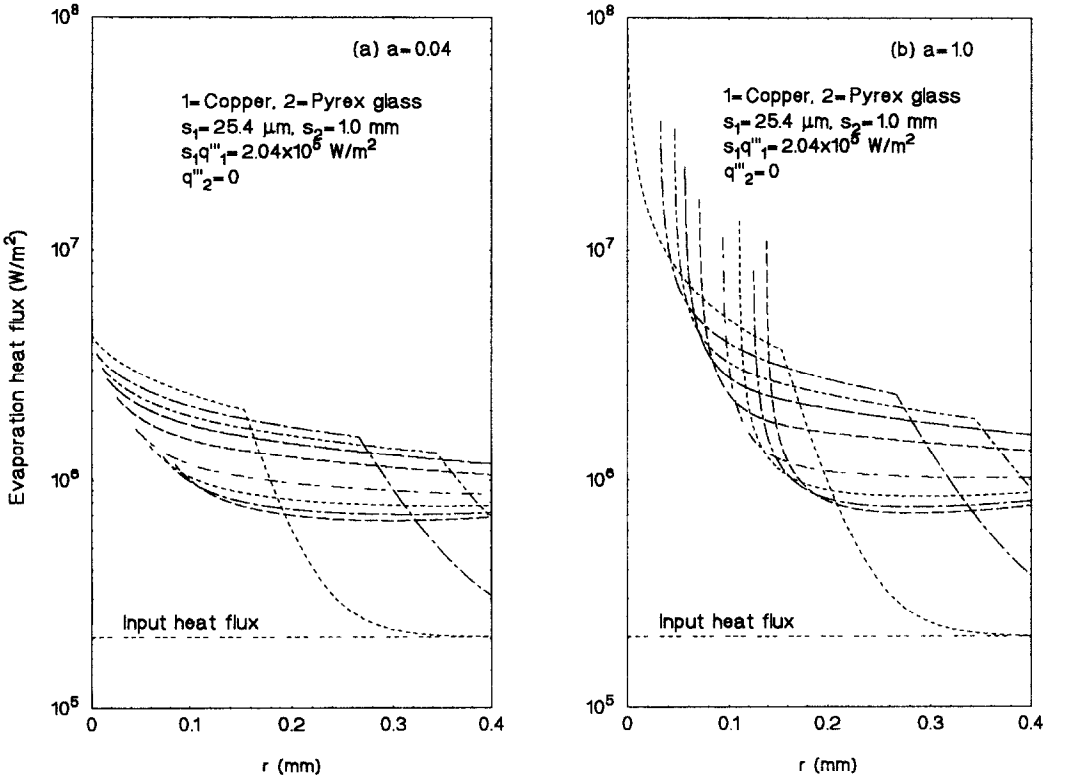

FIG. 7. Effect of the accommodation coefficient of evaporation on the evaporation heat flux on a heated copper wall.

the rate of evaporation shortly after the initiation of the microlayer evaporation. Figures 6 and 7 also show that the evaporation rate at the triple point is about one to two orders of magnitude higher than the input heat flux and its value at about 0.08 mm from the triple point. Beyond this point, the evaporation rate is almost uniform along the surface of the microlayer, but decreases with time as the liquid microlayer evaporation process continues. It should be noted that the evaporation heat flux in the microlayer away from the triple point is still about 5–10 times higher than the input heat flux. These results partially explain the high heat transfer rate associated with nucleate boiling and the observed rapid drop in the wall temperature in the heater during bubble growth [2, 3]. The very high evaporation rate at the triple point, which moves radially outward during the growth of the bubble, causes the local wall temperature to rapidly drop below the average temperature of the surface (see Fig. 5).

The effect of the accommodation coefficient on the evaporation rate of the microlayer can also be expressed in terms of the radius of the dry spot forming beneath the growing vapor bubble. Figures 8(a) and (b) compare the dry-spot radius on stainless-steel and copper surfaces for accommodation coefficients of 0.04 and 1.0 and a heater thickness of 25.4 and 10 μm, respectively. Note that a large difference in the dry-spot growth rate occurs during the early stage of the microlayer evaporation, when the stored heat in the heated wall is easily accessible. At a later stage, the growth of the dry-spot, and hence the evaporation rate, is dominated by the lateral conduction in the heated wall toward the triple point region, which depends on the thickness and thermal properties of the wall (Fig. 5).

Based on the results presented in Fig. 8, the microlayer evaporation process can be divided into two successive stages: evaporation dominated and conduction dominated stages. During the evaporation dominated stage, the surface heat flux is strongly dependent on the accommodation coefficient of evaporation and to a lesser extent on the lateral heat conduction in the heated wall. Figures 8(a) and (b) also show that not only the rate of evaporation, but also the duration of the evaporation dominated stage (as indicated by the changing slopes of the curves) depend on the thermal properties and the thickness of the heated wall.

As the evaporation of the liquid microlayer continues, the heat conduction in the wall begins to dominate the evaporation heat flux from the liquid microlayer. In this stage, the surface heat flux becomes less sensitive to the value of the accommodation coefficient, but strongly dependent on the thermal properties and/or the thickness of the heated wall. During this conduction controlled stage, the slopes of the curves in Fig. 8, which are significantly lower than during the earlier stage, are almost the same for a given wall material and wall thickness, regardless of the value of the accommodation coefficient. In

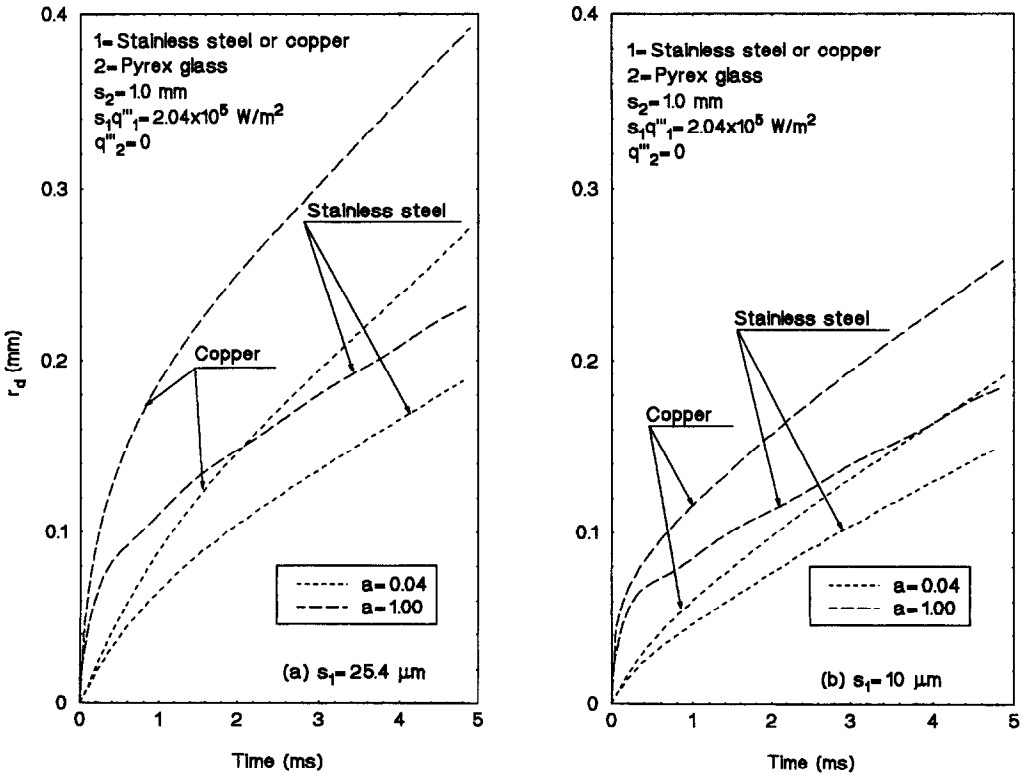

FIG. 8. Effect of the accommodation coefficient of evaporation on dry spot radius at different stages of bubble growth.

summary, during nucleate boiling the value of the accommodation coefficient of evaporation and both the thickness and thermal properties of the heated wall have a strong effect on the surface heat flux for the duration of the early stage of the bubble growth (less than 0.8 ms for cases presented in Fig. 8). In the subsequent stage, the time history of the bubble growth, and hence the evaporation rate are mainly controlled by lateral conduction in the heated wall.

4.4. *Effect of thickness and material of the heated wall*

Figure 9 shows the effects of the thickness and the material of the heated wall on the growth rate of the dry spot or the microlayer evaporation rate. In general, increasing the wall thickness increases the lateral heat conduction in the wall, resulting in a higher evaporation rate (or faster growth of the dry spot). Similarly, increasing lateral heat conduction by employing high conductivity material (for example Cu versus stainless-steel) also increases the microlayer evaporation rate. Note that the incremental increase in the evaporation rate as a result of increasing the wall thickness is larger for the high conductivity material.

Figure 9 also shows that for a 1.0 mm thick copper wall, the growth rate of the dry spot beneath the growing vapor bubble is solely controlled by the microlayer evaporation, regardless of the growth time. This is because, for such a high conductivity thick wall, the energy stored in the wall before the nucleation of the bubble as well as the low thermal resistance for lateral conduction provide all the heat needed for the evaporation of the microlayer at a rate approaching that for an isothermal wall. In this case, the microlayer evaporation is limited only by the liquid resistance and the value of the accommodation coefficient for evaporation. Similar observation can be made for a stainless-steel wall of the same thickness, however, because of its lower thermal conductivity, the radius of the dry spot is about half that in the case of Cu.

In the context of nucleate boiling, these results suggest that during the waiting period prior to bubble nucleation, the part of the heat input to the wall underneath a nucleation site is stored within the wall to raise its temperature. After a bubble nucleation, the previously stored heat as well as the heat input is drawn from the wall to vaporize the microlayer.

4.5. *Effect of lateral conduction within the heated wall*

The effect of lateral heat conduction within the heated or cooled wall is usually overlooked in most of the earlier analytical studies of boiling or condensation processes, respectively. In these studies, the wall surface has usually been assumed to be either isothermal or uniformly heated. However, as indicated in the previous section, the lateral conduction in the wall significantly affects the prediction of evaporation heat transfer rate. A high thermal conductivity wall (Cu for example) results in a higher evaporation rate and a faster dry spot growth rate, due to improved lateral heat conduction towards the s–l–v triple point region, than a low thermal conductivity wall. To demonstrate the effect of neglecting lateral conduction in the heated wall on the evaporation of a water microlayer, calculations are performed for a heated stainless-steel wall of variable thickness on a 1.0 mm thick Pyrex glass substrate. The calculated radius of the

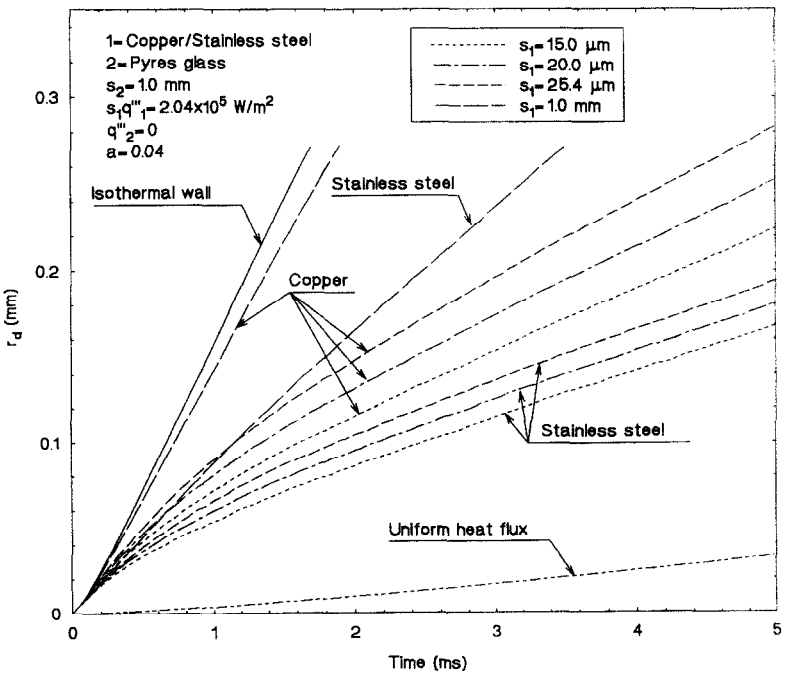

FIG. 9. Effects of the wall material and thickness on dry spot growth.

dry-spot, with and without lateral heat conduction in the wall, are compared in Fig. 9 as a function of time. The cases without lateral heat conduction are those assuming either an isothermal surface or an isoflux.

Results show that the predicted dry spot radius assuming an isoflux is only one fifth that predicted with the present model at the end of 5 ms for a stainless-steel wall that is 15 μm thick. For the same heated wall, the radius of the dry spot assuming an isothermal surface is more than three times that determined by the model with lateral conduction in the wall at the end of 1 ms. Therefore, the effect of lateral conduction in the heated wall is important when calculating the microlayer evaporation, and hence the heat transfer rate during nucleate boiling. Results in Fig. 9 suggest that while assuming an isoflux wall severely underestimates the radius of the dry spot, and hence the evaporation rate of the microlayer, assuming an isothermal wall overpredicts the radius of the dry spot for a thin or a low thermal conductivity wall, but is appropriate in the case of a thick or a high thermal conductivity wall.

To illustrate the lateral heat conduction in the heated wall, detailed temperature contours in the wall during microlayer evaporation are plotted in Fig. 10. This figure shows that a large temperature variation occurs within the wall and that the lowest temperature occurs near the solid–liquid–vapor contact region. The temperature contours clearly indicate that a lateral heat flow occurs towards the s–l–v region from both the dry spot area and the liquid covered area. The variations in the wall temperature with time for copper and stainless-steel walls are plotted in Figs. 11(a) and (b), respectively. Each curve in this figure represents the temperature variation with time at a certain radial distance (marked in mm) from the bubble nucleation site. Results show that the wall temperature during a bubble growth is far from isothermal, especially near the triple point where a temperature variation of as high as 9.5 K is calculated for an average input heat influx of 2.04×10^5 W m^{-2}.

In Fig. 11, the minima in the wall temperatures correspond to the location of the triple point. As this figure indicates, the triple point moves radially outward and the corresponding wall temperature decreases with time during the bubble growth. The drop in the surface temperature at the triple point is significantly higher for the low thermal conductivity (stainless-steel) wall than for the high thermal conductivity (copper) wall at the same time during the bubble growth. For example, at a radial location of 0.07 mm, the wall temperature corresponding to the triple point drops to about 50 and 90% of its initial value before bubble nucleation for a stainless-steel and a copper wall, respectively. These results clearly suggest that during nucleate boiling the temperature of the heated surface is highly non-uniform, which could introduce a large uncertainty in the experimental determination of the nucleate boiling heat flux. In order to reduce the experimental uncertainty, the heated wall thickness should be on the order of one millimeter or more (see Fig. 9), in order for lateral conduction in the wall to reduce the temperature drop associated with the movement of the triple point during bubble nucleation.

4.6. *Effect of a non-metallic coating on a metal substrate*

Enhancement of condensation heat transfer can be accomplished by coating a metal substrate with a thin layer of non-wetting, usually non-metallic material (for example, Teflon) to promote dropwise condensation. When a continuous condensate film is broken up into small drops, the overall condensation rate is

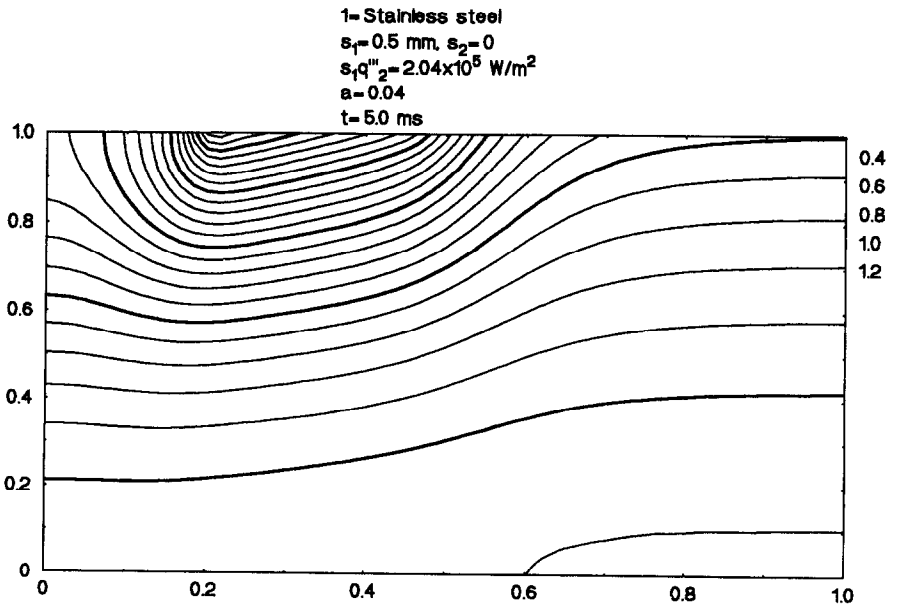

FIG. 10. Isotherms showing lateral heat conduction in the heated wall.

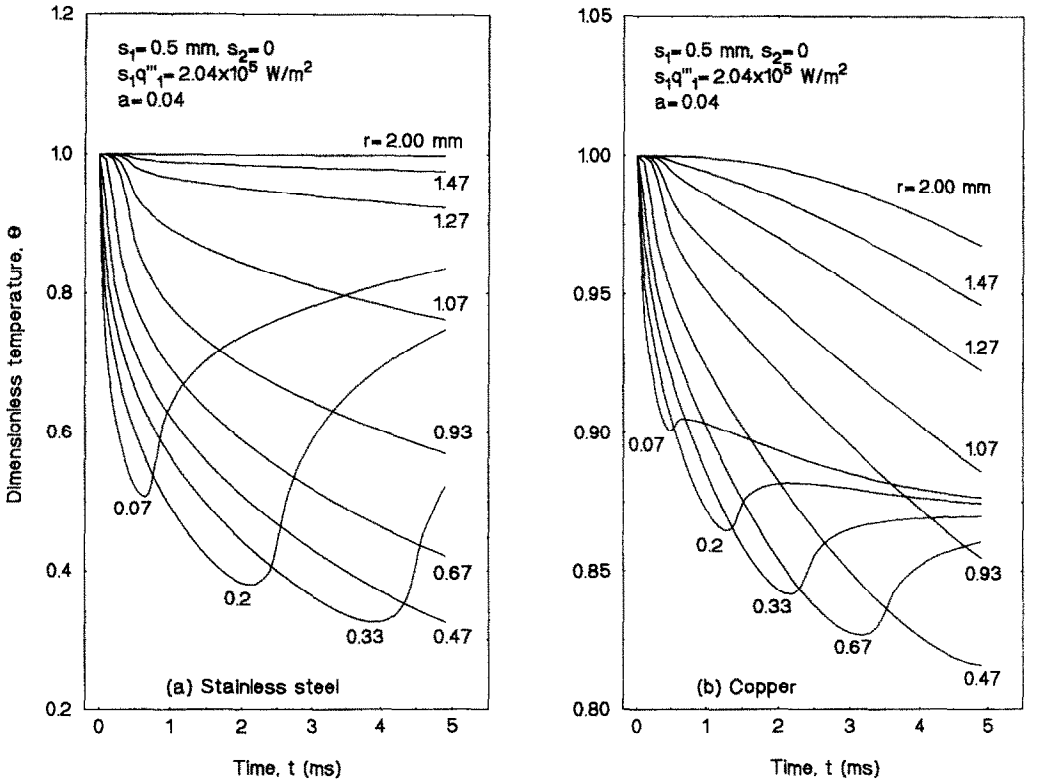

FIG. 11. Temperature variation of the liquid–solid interface.

augmented by the enhanced heat transfer rate at s-l-v triple point, which is made clear in the preceding discussion. However, since most of the non-metallic coating materials used have low thermal conductivities, they increase the thermal resistance to the heat transfer from the condensate to the cold metal substrate, and hence will affect the overall condensation heat transfer rate. However, the net effect of a non-metallic coating on the heat transfer rate will depend on its thickness and thermal properties as well as the thermal properties of the metal substrate.

In this section, the effect of a Pyrex glass coating on a copper substrate on the microlayer evaporation is investigated. Conclusions made can also be applied to dropwise condensation. Figure 12 shows the results for Pyrex glass coating of several thicknesses on a copper substrate of 1 mm thick. This figure clearly demonstrates the strong effect of the non-metallic coating on the growth of the dry spot beneath the growing bubble, and hence the microlayer evaporation rate. Compared to a uncoated copper wall (solid line in Fig. 12), a Pyrex glass coating of only 5 μm thick reduces the growth rate of the dry spot by as much as 37%, from about 139 to 88 mm s^{-1}. However, the incremental effect of increasing the thickness of the non-metallic coating decreases as the coating thickness increases. The significant reduction in the growth rate of the dry spot underneath the vapor bubble is indicative of the decrease in the evaporation heat transfer in the liquid microlayer. Therefore, in dropwise condensation application, the thickness of a non-metallic coating should be as thin as possible to avoid hindering the rate of heat transfer to the cold substrate, while maintaining its ability to promote dropwise condensation.

The effect of the non-metallic coating on the evaporation heat flux of the liquid microlayer is delineated in Figs. 13(a) and (b) for a 100 μm thick copper substrate. A comparison of the two figures indicates that the reduction in heat transfer rate due to a 5 μm thick glass coating is more significant in the triple point region, where the local surface heat flux experiences a reduction of 50%, in comparison to the uncoated surface. It should be noted that the non-metallic coating not only lowers the surface heat transfer rate, particularly at the triple point, but also makes it more uniform.

When a metallic substrate is coated with a non-metallic material, the effects of the thermal properties of the substrate metal on the microlayer evaporation depend very much on the thickness of the coating. In Figs. 14(a)–(c), the calculated dry-spot radius is plotted as a function of time to demonstrate the substrate effect. These figures show that the strongest effect of the substrate material on the microlayer evaporation occurs when there is no coating. The effect of the metal substrate becomes less significant as the coating thickness is increased, and eventually diminishes when the thickness of the Pyrex glass coating is equal to or greater than 20 μm.

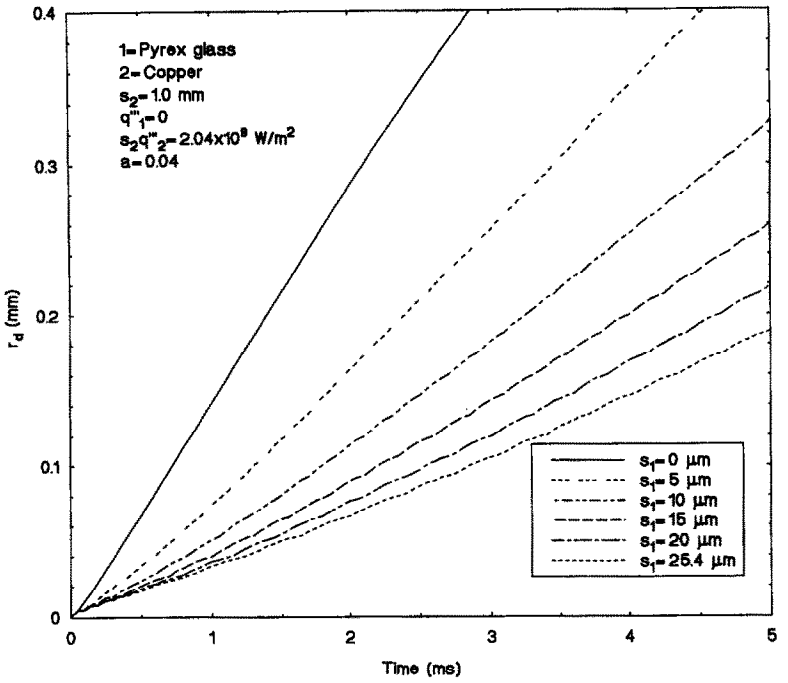

FIG. 12. Effect of the non-metallic coating thickness on a dry spot growth.

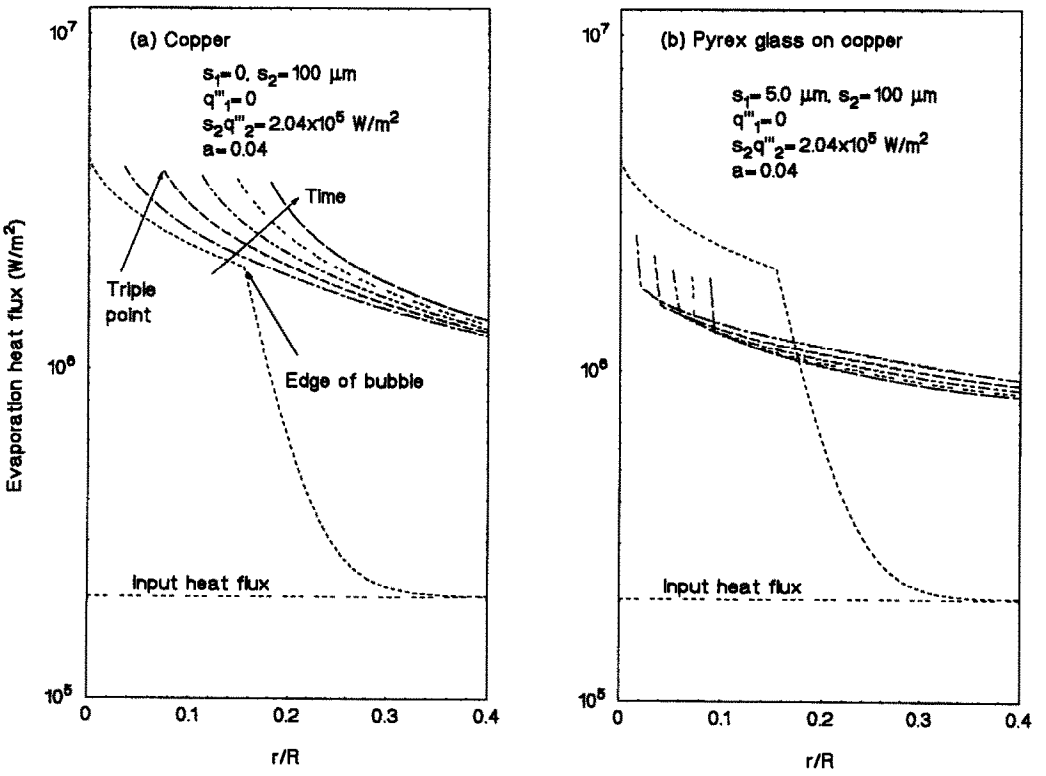

FIG. 13. Effect of a non-metallic coating on the microlayer evaporation heat flux.

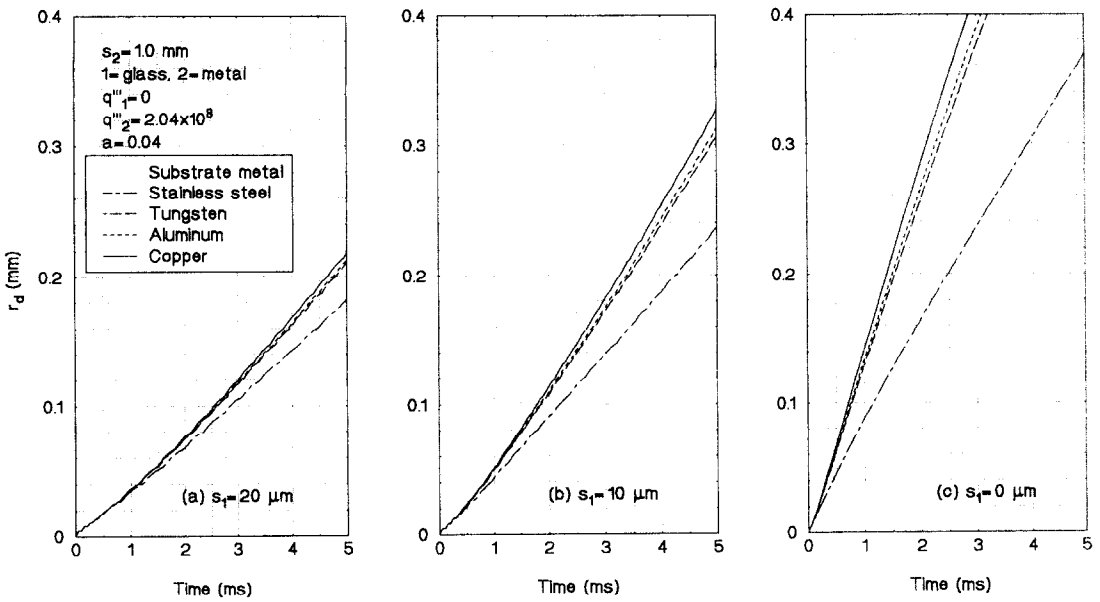

FIG. 14. Effects of the substrate thickness and material on microlayer evaporation.

5. SUMMARY AND CONCLUSIONS

Evaporation of a liquid microlayer under a growing vapor bubble on a flat surface of a composite wall is investigated. The wall consists of a thin, volumetrically heated metallic foil or film and a Pyrex glass substrate or thin coating. A transient model, which thermally couples the wall regions to the evaporating microlayer, is developed to simulate the microlayer evaporation. A parametric analysis is performed to investigate the effects of the wall composition, thickness and material properties, the value of accommodation coefficient of evaporation, and the waiting period between successive bubbles on microlayer evaporation. The model predictions are qualitatively in agreement with experimental data for a water microlayer evaporation on a SnO_2 coated Pyrex glass plate. The calculated transient axial and radial temperature distributions in the wall and the time histories of the local evaporation rate, microlayer thickness, and the radius of the dry spot underneath the bubble are presented and discussed.

Results show that in the case of a heated metal foil on a Pyrex glass substrate the local heat flux at the solid–liquid–vapor triple point could be as much as one to two orders of magnitude higher than the input heat flux, causing a significant drop in the wall temperature at the triple point. These results suggest that during nucleate boiling the temperature of the heated surface is highly non-uniform, which could introduce a large uncertainty in the experimental determination of the nucleate boiling heat flux. In order to reduce the experimental uncertainty, the thickness of the heated wall should be on the order of one millimeter or more. In this case, lateral conduction in the wall could reduce the temperature drop associated with the movement of the triple point during bubble nucleation.

The rate of microlayer evaporation increases as the thickness and thermal conductivity of the heated wall are increased due to improved lateral heat conduction. The values of the accommodation coefficient of evaporation as well as lateral conduction significantly affect the liquid microlayer evaporation on highly conductive wall, especially during the early stage of the transient. Conversely, a thin coating of a low conductivity material on a heated metal substrate significantly reduces the evaporation rate of the liquid microlayer and the effect of the heated metal substrate is negligible unless the coating is very thin.

Acknowledgements—This work was funded by the Institute for Space Nuclear Power Studies at the University of New Mexico.

REFERENCES

1. N. W. Snyder and D. K. Edward, Post conference comments, Summary of Conference on Bubble Dynamics and Boiling Heat Transfer Held at the Jet Propulsion Laboratory, JPL Memo No. 20–137 (1956).
2. F. D. Moore and R. B. Mesler, The measurement of rapid temperature fluctuations during nucleate boiling of water, *A.I.Ch.E. Jl* **7**, 620–624 (1961).
3. T. F. Rogers and R. B. Mesler, An experimental study of surface boiling by bubbles during nucleate boiling of water, *A.I.Ch.E. Jl* **10**, 656–660 (1964).
4. M. G. Cooper and A. J. P. Lloyd, Transient local heat flux in nucleate boiling, *Proc. Third Int. Heat Transfer Conf.*, Vol. 3, p. 193 (1966).
5. R. R. Sharp, The nature of liquid film evaporation during nucleate boiling, *NASA TN D*-1997 (1964).
6. C. M. Voutsinos and R. L. Judd, Laser interferometric investigations of the microlayer evaporation phenomenon, *J. Heat Transfer* **97**, 88–92 (1975).
7. L. D. Koffman and M. S. Plesset, Experimental observations of the microlayer in vapor bubble growth on a heated solid, *J. Heat Transfer* **105**, 625–632 (1983).
8. M. G. Cooper and A. J. P. Lloyd, The microlayer in

nucleate pool boiling, *Int. J. Heat Mass Transfer* **12,** 895–913 (1969).
9. L. A. Hale and S. A. Anderson, Surface temperatures and heat fluxes associated with the evaporation of a liquid film on a semi-infinite solid, *J. Heat Transfer* **93,** 357–364 (1971).
10. N. R. Prasad, J. S. Saini and R. Prakash, The effect of heater wall thickness on heat transfer in nucleate pool-boiling at high heat flux, *Int. J. Heat Mass Transfer* **28,** 1367–1375 (1985).
11. C. E. Brown and S. A. Martin, The effect of finite metal conductivity on the condensation heat transfer to falling water results on vertical heat-transfer surfaces, *J. Heat Transfer* **93,** 2627–2639 (1971).
12. Z. Guo and M. S. El-Genk, A study of liquid microlayer evaporation on a horizontal heated surface, Presented in the ASME Winter Annual Meeting, Atlanta, GA (1991).
13. M. Jacob and G. Hawkins, *Elements of Heat Transfer* (3rd Edn). Wiley, New York (1957).
14. Y. Y. Hsu and R. W. Graham, *Transport Processes in Boiling and Two-Phase Systems.* McGraw-Hill, New York (1976).
15. S. V. Patankar, *Numerical Heat Transfer and Fluid Flow.* Hemisphere, Washington, D.C. (1980).